Author Manuscript
Author Manuscript
Author Manuscript
Author Manuscript

HHS Public Access
Author manuscript
Dev Dyn. Author manuscript; available in PMC 2024 April 01.

Published in final edited form as:
Dev Dyn. 2023 April ; 252(4): 483–494. doi:10.1002/dvdy.555.

Frem1 activity is regulated by Sonic Hedgehog signaling in the cranial neural crest mesenchyme during midfacial morphogenesis

Matthew T. McLaughlin[1], **Miranda R. Sun**[1], **Tyler G. Beames**[1], **Austin C. Steward**[1], **Joshua W. M. Theisen**[2], **Hannah M. Chung**[1], **Joshua L. Everson**[1], **Ivan P. Moskowitz**[2], **Michael D. Sheets**[3], **Robert J. Lipinski**[1]

[1]Department of Comparative Biosciences, School of Veterinary Medicine, University of Wisconsin-Madison, Madison, WI, United States

[2]Department of Pediatrics, Pathology, Human Genetics and Genetic Medicine, The University of Chicago, Chicago, IL, United States

[3]Department of Biomolecular Chemistry, School of Medicine and Public Health, University of Wisconsin-Madison, Madison, WI, United States

Abstract

Background: Frem1 has been linked to human face shape variation, dysmorphology, and malformation, but little is known about its regulation and biological role in facial development.

Results: During midfacial morphogenesis in mice, we observed *Frem1* expression in the embryonic growth centers that form the median upper lip, nose, and palate. Expansive spatial gradients of *Frem1* expression in the cranial neural crest cell (cNCC) mesenchyme of these tissues suggested transcriptional regulation by a secreted morphogen. Accordingly, *Frem1* expression paralleled that of the conserved Sonic Hedgehog (Shh) target gene *Gli1* in the cNCC mesenchyme. Suggesting direct transcriptional regulation by Shh signaling, we found that *Frem1* expression is induced by SHH ligand stimulation or downstream pathway activation in cNCCs and observed GLI transcription factor binding at the *Frem1* transcriptional start site during midfacial morphogenesis. Finally, we found that FREM1 is sufficient to induce cNCC proliferation in a concentration-dependent manner and that Shh pathway antagonism reduces *Frem1* expression during pathogenesis of midfacial hypoplasia.

Conclusions: By demonstrating that the Shh signaling pathway regulates *Frem1* expression in cNCCs, these findings provide novel insight into the mechanisms underlying variation in midfacial morphogenesis.

Corresponding author: Robert J. Lipinski, Department of Comparative Biosciences, School of Veterinary Medicine, 2015 Linden Dr. Madison, WI 53706, Phone: (608) 265-4043, robert.lipinski@wisc.edu.

National Institute of Dental and Craniofacial Research: R00DE022010, R03DE027162
National Institute of Environmental Health Sciences: T32ES007015.

Author Manuscript Author Manuscript Author Manuscript Author Manuscript

Keywords

Frem/Fras; facial morphogenesis; facial dysmorphology; medial nasal processes; midface hypoplasia

Introduction

Substantial variation in facial morphology exists within and across human populations, and approximately one-third of all human birth defects involve craniofacial anomalies [1–3]. The Frem/Fras family of extracellular matrix proteins has been implicated in face shape variation and overt facial malformations. Mutations in human *FREM1*, *FREM2*, and *FRAS1* genes cause Manitoba-oculo-tricho-anal (MOTA), bifid nose with or without anorectal and renal anomalies (BNAR), and Fraser syndromes [4–6]. Craniofacial anomalies described in these syndromes include bifid nose, thin upper lip, shortened philtrum, and orofacial clefting [5,7–9]. Additionally, genome-wide association studies of human facial morphology have linked *FREM1* polymorphisms to shape variation of the central upper lip, while varying degrees of midfacial asymmetry and hypoplasia have been described in *Frem1* mutant mice [2,10–12]. Despite these genotype-phenotype relationships supported by both human and mouse studies, the regulatory mechanisms and roles of *Frem1* in facial morphogenesis have not been reported.

The biological activity of the Frem/Fras family has been most extensively characterized in epidermal development. FREM1 secreted by mesenchymal cells within the dermis is thought to form a ternary complex in the basement membrane with epidermally-secreted FREM2 and FRAS1 [13–15]. Disruption of this complex in cross-linking the epidermal basement membrane to the developing dermis manifests as a characteristic “blebbing” phenotype described in *Frem/Fras* mutant mice and related human syndromes [13,16]. However, an exclusive role in epidermal development is unlikely to explain the midfacial deficiency and dysmorphology linked to *Frem1* genetic variation.

In this study, we generated a detailed spatiotemporal expression profile of *Frem1* during mouse embryonic facial morphogenesis, defined upstream *Frem1* regulatory mechanisms, and examined downstream influences of FREM1 on cranial neural crest cell (cNCC) biology. We found that transcriptional regulation by Sonic Hedgehog (Shh) signaling establishes spatial gradients of *Frem1* in the cNCC mesenchyme, that FREM1 promotes concentration-dependent cNCC proliferation, and that Shh-Frem1 signaling is disrupted during pathogenesis of midface hypoplasia. These observations establish previously unrecognized regulators and roles of *Frem1* in cNCC biology that provide new insight into the mechanisms underlying variation in midfacial morphogenesis.

Results

Midfacial morphogenesis involves orchestrated outgrowth and fusion of paired facial growth centers (Fig. 1a-b) that are comprised of cNCC-derived mesenchyme covered by surface ectodermal epithelium (Fig. 1c-f). We applied microdissection, enzymatic separation, and qPCR to assess tissue-specific gene expression at gestational day (GD)11, when the medial

Author Manuscript Author Manuscript Author Manuscript Author Manuscript

nasal processes (MNPs) and the maxillary processes (MxPs) fuse bilaterally to close the upper lip in the mouse. In both of these tissues, *Frem2* and *Fras1* were predominantly detected in the epithelium, while *Frem1* expression was enriched in the mesenchyme (Fig. 1g-h). Whole-mount *in situ* hybridization revealed *Frem1* expression in the facial growth centers, with strong staining apparent in both the MNPs and MxPs (Fig. 1i). This was confirmed by staining of tissue sections, which revealed expansive spatial gradients of *Frem1* expression in MNP and MxP mesenchyme (Fig. 1j). *Frem2* expression was observed in the epithelium surrounding the growth centers and lining the entire nasal pit, while *Fras1* expression appeared limited to the epithelium on the medial aspect of the nasal pit (Fig. 1k-l).

The observed spatial gradient of *Frem1* expression prompted us to examine potential regulation by Sonic Hedgehog (SHH), a morphogen and critical regulator of facial development [17–19]. SHH ligand secreted by the facial ectodermal epithelium establishes a morphogen gradient that induces pathway activity in the cNCC mesenchyme [20], which can be visualized as expression of the conserved pathway target gene *Gli1.* We therefore examined expression of *Frem1* and *Gli1* at key stages of midfacial morphogenesis. *Frem1* and *Gli1* were expressed in spatial gradients in the cNCC-derived mesenchyme of the MNPs throughout their expansion from GD10.25 to GD11 (Fig. 2a-c, g-i). Gradients of *Frem1* and *Gli1* were also observed in the mesenchyme of the MxPs at GD10.25 and in MxP-derived palatal shelf mesenchyme and mandibular processes (MdP) at GD13 (Fig. 2d-f, j-l). In each of these domains, *Frem1* expression appeared restricted to the mesenchyme and within the domains of *Gli1* expression.

We next examined whether Shh signaling directly regulates *Frem1* expression in a mouse cNCC line (O9–1) that recapitulates the expression signature and differentiation capacity of *in vivo* multipotent cNCCs [21]. Stimulation of cultured cNCCs with SHH ligand significantly increased the expression of both *Gli1* and *Frem1* compared to vehicle alone (Fig. 3a-b). The SHH ligand-induced expression of both *Gli1* and *Frem1* was blocked by exposure to vismodegib, a specific inhibitor of the obligate Shh pathway signal transducing protein Smoothened (SMO) [22]. We therefore tested whether genetic and pharmacologic activation of SMO could directly regulate *Frem1* expression. Overexpression of a constitutively active form of human *SMO* in cultured cNCCs resulted in significantly increased *Gli1* and *Frem1* expression (Fig. 3c-d). Accordingly, acute pathway activation via addition of the small molecule SMO activator SAG was sufficient to upregulate *Gli1* and *Frem1* expression (Fig. 3e-f). *Frem2* expression was not detected in cultured cNCCs (not shown).

Our observations from *in vivo* development and cNCC culture suggested transcriptional regulation of *Frem1* by the Shh signaling pathway. Three zinc-finger GLI proteins, GLI1, GLI2, and GLI3, regulate transcription of Shh target genes. Each of the three GLI transcription factor family members contain five zinc-finger domains and recognize a common consensus sequence [23–26]. To assess GLI binding sites in the developing face, we utilized a published mouse GLI3 ChIP-seq data set generated from GD11.5 whole face tissue, including the MNPs and MxPs [27]. ChIP-seq revealed binding of GLI3 at the transcription start sites of *Frem1*, while minimal to no signal was apparent near *Frem2* or *Frem3* (Fig. 4a-c). Established Shh-Gli transcriptional targets in cNCCs during facial

Author Manuscript Author Manuscript Author Manuscript Author Manuscript

development, including *Gli1*, *Ccnd2*, and *Foxf2* (Fig. 4d-f), showed GLI3 ChIP-seq signal comparable to that of *Frem1* [18,24,28,29].

We next assessed the influence of FREM1 on cNCC migration and proliferation. After undergoing epithelial-to-mesenchymal transition, cNCCs migrate away from the dorsal margins of the neural folds into the field of facial morphogenesis, then rapidly proliferate to form the mesenchyme of the facial growth centers. To assess migration, scratch assays were conducted with cNCCs cultured in the absence or presence of recombinant human FREM1 protein. FREM1 is highly conserved between humans and mice, exhibiting 85% homology [15,30]. No significant impact of FREM1 was observed on the width of the scratches over time (Fig. 5a-g). The potential influence on proliferation was then examined by culturing cNCCs in the absence or presence of graded concentrations of FREM1 for 24 hours, with EdU added to culture media for the last 2 hours. Addition of FREM1 resulted in a concentration-dependent increase in EdU incorporation (Fig. 5h-j), with the highest tested FREM1 concentration of 7.5 μg/ml resulting in a 20% increase.

Frem1 mutant mice exhibit varying degrees of midfacial hypoplasia and asymmetry [10]. We have previously demonstrated that *in utero* antagonism of the Shh signaling pathway reduces cNCC proliferation, attenuating MNP outgrowth and resulting in a spectrum of related phenotypic outcomes ranging from midfacial hypoplasia to cleft lip (Fig. 6a-c) [18,31]. We therefore examined the impact of Shh pathway antagonism on *Frem1* expression during the pathogenesis of midfacial hypoplasia/cleft lip. Embryos were exposed to the Shh pathway inhibitor cyclopamine (or vehicle alone) using an exposure paradigm that targets post-migrational cNCCs [18,32]. Frontonasal prominence (FNP) tissue that gives rise to the paired medial and lateral nasal processes was isolated by microdissection from GD9.25 embryos, and gene expression was assessed by qPCR. Expression levels of both *Gli1* and *Frem1* were significantly reduced in FNP tissue of embryos exposed to cyclopamine compared to vehicle alone (Fig. 6d). Cyclopamine treatment did not significantly impact expression of *Frem2* or *Fras1.* Spatial gene expression was then examined on a parallel cohort of embryos collected at GD10, when the MNPs are undergoing initial outgrowth. Consistent with observations shown in Fig. 2, both *Frem1* and *Gli1* were expressed in spatial gradients in the MNP mesenchyme of vehicle-exposed embryos (Fig. 6e, g). In embryos exposed to the Shh pathway antagonist cyclopamine, mesenchymal expression of both *Gli1* and *Frem1* was markedly diminished in the mesenchyme of the MNP region (Fig. 6f, h).

Discussion

This study is the first to demonstrate that *Frem1* is regulated by the Shh signaling pathway, a key driver of facial morphogenesis [20,33]. Previous studies have described *Frem1* expression in restricted domains localized to sites of epithelial-mesenchymal interaction in several developmental contexts [5,15]. In the embryonic facial growth centers, we observed expansive *Frem1* spatial gradients that parallel *Gli1,* a reliable indicator of Shh pathway activity. The canonical Shh signaling pathway is initiated by SHH ligand binding to the transmembrane protein PTCH1, relieving its repression of SMO, which then localizes to the primary cilium and triggers a downstream signaling cascade culminating in transcriptional regulation of pathway target genes by the GLI transcription factor family. We found that

Author Manuscript Author Manuscript Author Manuscript Author Manuscript

SHH ligand-stimulated upregulation of *Frem1* can be blocked by SMO inhibition and that genetic or pharmacologic SMO activation is sufficient to induce *Frem1* expression. Leveraging a previously published GLI3 ChIP-seq data set [27], we also found evidence of GLI transcription factor binding at the *Frem1* promoter *in vivo*. Taken together, these findings suggest that *Frem1* expression is directly regulated by canonical Shh-Gli signaling during midfacial morphogenesis.

The Shh-Frem1 regulatory relationship revealed in this study contextualizes *Frem1*-associated facial phenotypes with those resulting from Shh pathway inhibition. Mutations in *FREM1* result in BNAR syndrome (OMIM #608980) and MOTA syndrome (OMIM #248450). Facial features described in affected individuals include bifid or bulbous nasal tip, short philtrum, thin upper lip, highly arched palate, and upper incisor abnormalities [4,5,34–36]. *FREM1* polymorphisms have also been linked to shape variation of the central upper lip [2,11]. These outcomes are consistent with the prominent gradients of *Frem1* observed during expansion of the MNPs, which form the median aspect of the nose, including the nasal septum and nasal tip, the upper lip philtrum, and the central portion of the alveolar ridge that contains the upper central incisors. Expansion of the MNPs is dependent upon Shh signaling and highly sensitive to pathway disruption [31]. Human mutations in *SHH* and other genes encoding pathway effectors are associated with holoprosencephaly, a malformation of the developing forebrain. Reflecting the requirement of Shh activity in the development of the forebrain and adjacently developing face, the prosencephalic anomalies that define holoprosencephaly co-occur with midfacial deficiency manifesting as severe hypoplasia, median and lateral orofacial clefts, highly arched palate, and a single central incisor [37–39]. These comparisons suggest that disruption of *Frem1* itself results in outcomes that fall within, but are generally less severe than, those caused by complete Shh pathway inhibition. This premise is further supported by our observation that *Frem1* expression is reduced following Shh pathway inhibition and during pathogenesis of midfacial hypoplasia/cleft lip. *Frem1* then appears to be one of several Shh pathway target genes, including previously identified members of the Forkhead box transcription factor family, that influence cNCC biology and are individually required for midfacial morphogenesis [18,20].

The evidence presented herein and in previous reports suggests some degree of specificity to Shh pathway regulation of *Frem1*. In addition to the developing face, cNCCs also form the mesenchyme of several cranial sutures. Shh signaling is required to maintain stem cell activity in the mesenchymal suture niche, and metopic craniosynostosis has been observed following ablation of *Gli1* positive cells in the suture or following systemic Shh pathway inhibition [31,40] Interestingly, *Frem1* is also expressed in the metopic suture and craniosynostosis has been observed in *Frem1* mutant mice as well as individuals with heterozygous *FREM1* mutations [10]. These observations suggest that Shh signaling may regulate *Frem1* in cNCCs in multiple developmental contexts. However, this regulatory relationship does not appear to be conserved across all cell types and developmental contexts. For example, Shh signaling plays critical roles in prosencephalic development, and *Gli1* is expressed in specific domains of the diencephalon and telencephalon [33,41]. While we observed *Gli1* in these well-established domains of pathway activity in the neuroectoderm, *Frem1* expression was not detected in the neuroectoderm (Figs 2 and 6). Moreover, while genetic and chemical disruption of the Shh pathway causes midface anomalies that co-occur

Author Manuscript Author Manuscript Author Manuscript Author Manuscript

with characteristic and severe forebrain malformation, no reports have described forebrain anomalies in humans or mice with *Frem1* mutations. Known roles of Shh signaling also do not readily correspond to the diaphragmatic and kidney malformations described to result from *Frem1* disruption [42,43]. While Shh signaling and *Frem1* play functional roles in skin and anorectal development, whether *Frem1* is a downstream effector of Shh signaling in these contexts is not known [12,15,44–46]. Taken together, these observations suggest that *Frem1* transcriptional regulation by the Shh signaling pathway is not universal but limited to specific contexts. Determining the mechanism of this apparent regulatory specificity will require further investigation.

Frem1 has been demonstrated to have multiple context-dependent roles during development. Apart from complexing with FREM2 and FRAS1 in dermis-epidermis adhesion, studies have identified a role for FREM1 in mesenchymal proliferation during mammalian diaphragm development and primary mesenchymal cell migration in sea urchin development [43,47]. These biological processes are also required for cNCC development and facial morphogenesis. cNCCs are specified at the dorsal margins of the anterior neural folds, undergo epithelial-to-mesenchymal transition, migrate extensively, and then rapidly proliferate to form the majority of the connective tissue of the head and face. Disruptions in cNCC migration and proliferation contribute to facial malformations and dysmorphology [48,49]. While not overtly impacting cNCC migration in the scratch assay, we found that addition of FREM1 to cNCCs resulted in a concentration-dependent increase in proliferation (Fig. 5). The concentration-dependence of this effect is notable given the regulation of *Frem1* by a secreted morphogen and the spatial gradient of *Frem1* expression during facial morphogenesis. Our finding that FREM1 promotes post-migrational cNCC proliferation provides a plausible cellular mechanism for the midfacial variation and dysmorphology associated with human *FREM1* variants and midfacial deficiency observed in *Frem1* mutant mice [10]. The previous study demonstrating a role for Frem1 in promoting mesenchymal proliferation in diaphragm development found no impact on apoptosis, though this endpoint was not examined in the present study. Therefore, how Frem1 influences the balance of proliferation and apoptosis in cNCC mesenchyme during facial morphogenesis will need to be addressed in future studies.

The findings presented in this study reveal *Frem1* regulation as a novel mechanism by which Shh signaling controls facial morphogenesis. These results provide a developmental framework to understand *FREM1*-associated facial variation and the relationship of these outcomes to those resulting from genetic or environmental disruption of the Shh signaling pathway. These findings expand our understanding of the mechanisms that regulate facial morphogenesis and how their disruption contributes to human face shape variation and facial malformations.

Experimental Procedures

Animal studies:

This study was conducted in strict accordance with the recommendations in the Guide for the Care and Use of Laboratory Animals of the National Institutes of Health. The protocol was approved by the University of Wisconsin School of Veterinary Medicine Institutional

Author Manuscript Author Manuscript Author Manuscript Author Manuscript

Animal Care and Use Committee (Protocol No. 13–081.0). C57BL/6J mice were purchased from The Jackson Laboratory and housed under specific pathogen-free conditions in disposable, ventilated cages (Innovive, San Diego, CA). Rooms were maintained at 22 ± 2 °C and 30–70% humidity on a 12-hour light, 12-hour dark cycle. Mice were fed 2920× Irradiated Harlan Teklad Global Soy Protein-Free Extruded Rodent Diet until day of plug, when dams received 2919 Irradiated Teklad Global 19% Protein Extruded Rodent Diet. One or two nulliparous female mice were placed with a single male for 1–2 hours and then examined for copulation plugs. The beginning of the mating period was designated as gestational day (GD)0, and pregnancy was confirmed by assessing weight gain between GD7 and GD10, as previously described [50].

Pregnant dams were administered 90 mg/kg/day cyclopamine (LC Laboratories, CAS #4449–51-8) or vehicle alone from GD8.25 to approximately GD9.375 by subcutaneous infusion exposure using ALZET 2001D micro-osmotic pumps (Cupertino, CA, United States) as previously described [18,32]. Pregnant dams were euthanized by carbon dioxide inhalation followed by cervical dislocation for embryo collection. Separation of mesenchyme and surface ectodermal epithelium of GD11 medial nasal processes and maxillary processes was accomplished as previously described [18,51]. Tissues from an entire litter were pooled, and N=4 litters were used for RNA expression analyses. GD9.25 frontonasal prominence (FNP) tissue was microdissected and pooled as previously described [18]. N=6 litters for each treatment group were used for RNA expression analyses.

In situ hybridization:

Embryos at GD10, 10.25, 11, and 13 were dissected in PBS and fixed in 4% paraformaldehyde for 18 hours. Embryos then underwent graded dehydration (1:3, 1:1, 3:1 v/v) into 100% methanol and were stored at −20°C indefinitely for subsequent ISH analysis. Rehydrated embryos were embedded in 4% agarose gel and cut in 50 μm sections using a vibrating microtome. ISH was performed as previously described [41]. Sections were imaged using a MicroPublisher 5.0 camera connected to an Olympus SZX-10 stereomicroscope. Gene-specific ISH riboprobe primers were designed using IDT PrimerQuest and affixed with the T7 polymerase consensus sequence plus a 5-bp leader sequence to the reverse primer. Sequences are listed in Table 1.

Cell culture:

Immortalized O9–1 cranial neural crest cells were provided by Dr. Robert Maxson, Keck School of Medicine at the University of Southern California, and cultured as described by Ishii and colleagues [21]. O9–1 cell lines stably overexpressing GFP or a constitutively active form of Smoothened (SMO^{M2}) were generated as previously described [18].

Gene expression analysis:

O9–1 cells were plated at 5×10^5 cells/mL (0.4 mL per well in a 24-well plate) and were allowed to attach in complete O9–1 media for 24 hours. Media were replaced with DMEM containing 1% FBS and treatments of ± 0.4 μg/mL SHH ligand (R&D Systems) ± 100 nM vismodegib (LC Laboratories) or ± 50 nM Smoothened Agonist (LC Laboratories). Cells were harvested at 48 hours following treatment for RNA extraction. N=5 biological

Author Manuscript Author Manuscript Author Manuscript Author Manuscript

replicates were used in each treatment group. RNA was isolated from cells grown *in vitro* and from embryonic tissue using the Illustra RNAspin kit according to the manufacturer recommendations with on-column DNase digestion. cDNA was synthesized from 100–500 ng of total RNA using the GoScript reverse transcription reaction kits (Promega). Singleplex quantitative real-time polymerase chain reaction (qPCR) was performed using SSoFast EvaGreen Supermix (Bio-Rad) on a Bio-Rad CFX96 real-time PCR detection system (Bio-Rad Laboratories, Hercules, CA). qPCR primers were designed using PrimerQuest (IDT), and sequences are listed in Table 2. Target gene specificity was confirmed using National Center for Biotechnology Information Primer-Basic Local Alignment Search Tool (NCBI Primer-BLAST). *Gapdh* was used as the housekeeping gene, and analyses were conducted with the 2-ΔΔCt method.

GLI binding site analyses:

To identify GLI binding sites in the developing face, published FLAG ChIP-seq data from *Gli3*^{3XFlag} knock-in mice were accessed from GEO record GSE146961 [27,52]. Raw sequencing reads were aligned to the mm10 genome using Bowtie2 and SAMtools [53] and filtered for a minimum mapping quality of 10 (-q 10). Fold-enrichment tracks were generated with BEDTools (v2.30.3) using the genomecov and bedGraphToBigWig functions [54]. Tracks were then visualized with the IGV genome browser (v2.4.14) [55] and edited with Adobe Illustrator (Adobe Inc., San Jose, CA).

Migration assays:

O9–1 cells were plated at 5×10^5 cells/mL (0.4 mL per well in a 24-well plate) and allowed to attach in complete O9–1 media for 16 h. Immediately prior to beginning treatments, each well was scratched with a sterile 200 μL pipet tip vertically and washed twice with DPBS. Recombinant FREM1 protein (R&D Systems, Minneapolis, MN) dissolved in DPBS was diluted to final concentrations of 7.5 μg/mL, 2.5 μg/mL, and 0.83 μg/mL in DMEM containing 1% FBS, and 400 μL treatment or DPBS vehicle media were added to each well. Phase contrast images were taken with a MicroPublisher 5.0 camera (QImaging, Tucson, AZ) mounted on a Nikon Eclipse TS100 (Nikon Instruments Inc., Melville, NY) using a 4× objective every hour for 8 hours following the initiation of the treatment period. Migration rate was assessed using ImageJ. Experiments were performed in biological triplicate.

Proliferation assays:

O9–1 cells were plated at 5×10^4 cells/mL (0.4 mL per well in a 24-well plate) in Matrigel-coated wells and allowed to attach in complete O9–1 media for 16 h. Recombinant FREM1 protein (R&D Systems, Minneapolis, MN) dissolved in DPBS was diluted to final concentrations of 7.5 μg/mL, 2.5 μg/mL, and 0.83 μg/mL in DMEM containing 1% FBS, and 400 μL treatment or DPBS vehicle media were added to each well. At 22 h post-treatment, half of the media were removed from each well and replaced with a 2× solution of EdU (Invitrogen, Waltham, MA), per the manufacturer's recommendations. Cells were incubated in the EdU solution for 2 hours prior to fixation in 4% paraformaldehyde for 15 min. EdU and Hoechst staining were performed according to the manufacturer's instructions with volumes adjusted for use in a 24-well plate. Fluorescent images were captured using the Keyence BZ-X700 fluorescent microscope (Keyence, Itasca, IL), and

Author Manuscript Author Manuscript Author Manuscript Author Manuscript

Hoechst+ and EdU+ cells were counted in 4 non-adjacent fields per well using Keyence BZ-X Image Analysis software. Experiments were performed in technical duplicate for a total of N=3 biological replicates.

Statistics:

One-way analysis of variance (ANOVA) with Tukey's post hoc test or two-tailed t-tests, where appropriate, were used to determine whether gene expression was changed in cultured cNCCs and in microdissected FNP tissue. ANOVA with Dunnett's post hoc test for multiple comparisons was used for analyses of cNCC migration and proliferation assays. GraphPad Prism 6 was used for all statistical analyses. An alpha value of 0.05 was maintained for determination of significance.

Acknowledgments

Research reported in this publication was supported by the National Institute of Dental and Craniofacial Research and the National Institute of Environmental Health Sciences of the National Institutes of Health under award numbers R00DE022010, R03DE027162, and T32ES007015. The content is solely the responsibility of the authors and does not necessarily represent the official views of the National Institutes of Health. Support was also provided by a University of Wisconsin Hilldale Undergraduate Research Award. The authors thank Drs. Ian Smyth, Daryl Scott, and Kiyotoshi Sekiguchi for their generous willingness to share reagents and Dr. Suzanne Ponik for helpful discussion.

References

1. Cox TC, Luquetti DV, Cunningham ML. Perspectives and challenges in advancing research into craniofacial anomalies. Am J Med Genet C Semin Med Genet Nov 2013;163C(4):213–7. 10.1002/ajmg.c.31383. [PubMed: 24142870]
2. White JD, Indencleef K, Naqvi S, et al. Insights into the genetic architecture of the human face. Nat Genet 01 2021;53(1):45–53. 10.1038/s41588-020-00741-7. [PubMed: 33288918]
3. Matthews HS, Palmer RL, Baynam GS, et al. Large-scale open-source three-dimensional growth curves for clinical facial assessment and objective description of facial dysmorphism. Sci Rep 06 09 2021;11(1):12175. 10.1038/s41598-021-91465-z. [PubMed: 34108542]
4. Slavotinek AM, Baranzini SE, Schanze D, et al. Manitoba-oculo-tricho-anal (MOTA) syndrome is caused by mutations in FREM1. J Med Genet Jun 2011;48(6):375–82. 10.1136/jmg.2011.089631. [PubMed: 21507892]
5. Alazami AM, Shaheen R, Alzahrani F, et al. FREM1 mutations cause bifid nose, renal agenesis, and anorectal malformations syndrome. Am J Hum Genet Sep 2009;85(3):414–8. 10.1016/j.ajhg.2009.08.010. [PubMed: 19732862]
6. McGregor L, Makela V, Darling SM, et al. Fraser syndrome and mouse blebbed phenotype caused by mutations in FRAS1/Fras1 encoding a putative extracellular matrix protein. Nat Genet Jun 2003;34(2):203–8. 10.1038/ng1142. [PubMed: 12766769]
7. Gattuso J, Patton MA, Baraitser M. The clinical spectrum of the Fraser syndrome: report of three new cases and review. J Med Genet Sep 1987;24(9):549–55. 10.1136/jmg.24.9.549. [PubMed: 3118036]
8. Chacon-Camacho OF, Zenker M, Schanze D, Ledesma-Gil J, Zenteno JC. Novel FREM1 mutations in a patient with MOTA syndrome: Clinical findings, mutation update and review of FREM1-related disorders literature. Eur J Med Genet Mar 2017;60(3):190–194. 10.1016/j.ejmg.2017.01.005. [PubMed: 28111185]
9. Slavotinek AM, Tifft CJ. Fraser syndrome and cryptophthalmos: review of the diagnostic criteria and evidence for phenotypic modules in complex malformation syndromes. J Med Genet Sep 2002;39(9):623–33. 10.1136/jmg.39.9.623. [PubMed: 12205104]

Author Manuscript Author Manuscript Author Manuscript Author Manuscript

10. Vissers LE, Cox TC, Maga AM, et al. Heterozygous mutations of FREM1 are associated with an increased risk of isolated metopic craniosynostosis in humans and mice. PLoS Genet Sep 2011;7(9):e1002278. 10.1371/journal.pgen.1002278. [PubMed: 21931569]
11. Lee MK, Shaffer JR, Leslie EJ, et al. Genome-wide association study of facial morphology reveals novel associations with FREM1 and PARK2. PLoS One 2017;12(4):e0176566. 10.1371/journal.pone.0176566. [PubMed: 28441456]
12. Beck TF, Shchelochkov OA, Yu Z, et al. Novel frem1-related mouse phenotypes and evidence of genetic interactions with gata4 and slit3. PLoS One 2013;8(3):e58830. 10.1371/journal.pone.0058830. [PubMed: 23536828]
13. Kiyozumi D, Sugimoto N, Sekiguchi K. Breakdown of the reciprocal stabilization of QBRICK/Frem1, Fras1, and Frem2 at the basement membrane provokes Fraser syndrome-like defects. Proc Natl Acad Sci U S A Aug 08 2006;103(32):11981–6. 10.1073/pnas.0601011103. [PubMed: 16880404]
14. Petrou P, Chiotaki R, Dalezios Y, Chalepakis G. Overlapping and divergent localization of Frem1 and Fras1 and its functional implications during mouse embryonic development. Exp Cell Res Mar 10 2007;313(5):910–20. 10.1016/j.yexcr.2006.12.008. [PubMed: 17240369]
15. Smyth I, Du X, Taylor MS, Justice MJ, Beutler B, Jackson IJ. The extracellular matrix gene Frem1 is essential for the normal adhesion of the embryonic epidermis. Proc Natl Acad Sci U S A Sep 14 2004;101(37):13560–5. 10.1073/pnas.0402760101. [PubMed: 15345741]
16. Smyth I, Scambler P. The genetics of Fraser syndrome and the blebs mouse mutants. Hum Mol Genet Oct 15 2005;14 Spec No. 2:R269–74. 10.1093/hmg/ddi262.
17. Heyne GW, Melberg CG, Doroodchi P, et al. Definition of critical periods for Hedgehog pathway antagonist-induced holoprosencephaly, cleft lip, and cleft palate. PLoS One 2015;10(3):e0120517. 10.1371/journal.pone.0120517. [PubMed: 25793997]
18. Everson JL, Fink DM, Yoon JW, et al. Sonic hedgehog regulation of Foxf2 promotes cranial neural crest mesenchyme proliferation and is disrupted in cleft lip morphogenesis. Development Jun 2017;144(11):2082–2091. 10.1242/dev.149930. [PubMed: 28506991]
19. Kurosaka H. The Roles of Hedgehog Signaling in Upper Lip Formation. Biomed Res Int 2015;2015:901041. 10.1155/2015/901041. [PubMed: 26425560]
20. Jeong J, Mao J, Tenzen T, Kottmann AH, McMahon AP. Hedgehog signaling in the neural crest cells regulates the patterning and growth of facial primordia. Genes Dev Apr 15 2004;18(8):937–51. 10.1101/gad.119030418/8/937 [pii]. [PubMed: 15107405]
21. Ishii M, Arias AC, Liu L, Chen YB, Bronner ME, Maxson RE. A stable cranial neural crest cell line from mouse. Stem Cells Dev Nov 2012;21(17):3069–80. 10.1089/scd.2012.0155. [PubMed: 22889333]
22. Robarge KD, Brunton SA, Castanedo GM, et al. GDC-0449-a potent inhibitor of the hedgehog pathway. Bioorg Med Chem Lett Oct 2009;19(19):5576–81. 10.1016/j.bmcl.2009.08.049. [PubMed: 19716296]
23. Kinzler KW, Vogelstein B. The GLI gene encodes a nuclear protein which binds specific sequences in the human genome. Mol Cell Biol Feb 1990;10(2):634–42. [PubMed: 2105456]
24. Yoon JW, Kita Y, Frank DJ, et al. Gene expression profiling leads to identification of GLI1-binding elements in target genes and a role for multiple downstream pathways in GLI1-induced cell transformation. J Biol Chem Feb 2002;277(7):5548–55. 10.1074/jbc.M105708200. [PubMed: 11719506]
25. Vokes SA, Ji H, McCuine S, et al. Genomic characterization of Gli-activator targets in sonic hedgehog-mediated neural patterning. Development May 2007;134(10):1977–89. 10.1242/dev.001966. [PubMed: 17442700]
26. Peterson KA, Nishi Y, Ma W, et al. Neural-specific Sox2 input and differential Gli-binding affinity provide context and positional information in Shh-directed neural patterning. Genes Dev Dec 15 2012;26(24):2802–16. 10.1101/gad.207142.112. [PubMed: 23249739]
27. Elliott KH, Chen X, Salomone J, et al. Gli3 utilizes Hand2 to synergistically regulate tissue-specific transcriptional networks. Elife 10 02 2020;9. 10.7554/eLife.56450.

Author Manuscript Author Manuscript Author Manuscript Author Manuscript

28. Mill P, Mo R, Fu H, et al. Sonic hedgehog-dependent activation of Gli2 is essential for embryonic hair follicle development. Genes Dev Jan 15 2003;17(2):282–94. 10.1101/gad.1038103. [PubMed: 12533516]
29. Lan Y, Jiang R. Sonic hedgehog signaling regulates reciprocal epithelial-mesenchymal interactions controlling palatal outgrowth. Development Apr 2009;136(8):1387–96. https://doi.org136/8/1387 [pii] 10.1242/dev.028167. [PubMed: 19304890]
30. Kiyozumi D, Osada A, Sugimoto N, et al. Identification of a novel cell-adhesive protein spatiotemporally expressed in the basement membrane of mouse developing hair follicle. Exp Cell Res May 15 2005;306(1):9–23. 10.1016/j.yexcr.2005.01.020. [PubMed: 15878328]
31. Lipinski RJ, Song C, Sulik KK, et al. Cleft lip and palate results from Hedgehog signaling antagonism in the mouse: Phenotypic characterization and clinical implications. Birth Defects Res A Clin Mol Teratol Apr 2010;88(4):232–40. 10.1002/bdra.20656. [PubMed: 20213699]
32. Lipinski RJ, Hutson PR, Hannam PW, et al. Dose-and route-dependent teratogenicity, toxicity, and pharmacokinetic profiles of the hedgehog signaling antagonist cyclopamine in the mouse. Toxicological sciences 2008;104(1):189–197. [PubMed: 18411234]
33. Marcucio RS, Cordero DR, Hu D, Helms JA. Molecular interactions coordinating the development of the forebrain and face. Dev Biol Aug 2005;284(1):48–61. 10.1016/j.ydbio.2005.04.030. [PubMed: 15979605]
34. Brischoux-Boucher E, Dahlen E, Gronier C, et al. Bifid nose as the sole manifestation of BNAR syndrome, a FREM1-related condition. Clin Genet 11 2020;98(5):515–516. 10.1111/cge.13821. [PubMed: 32926405]
35. Al-Gazali LI, Bakir M, Hamud OA, Gerami S. An autosomal recessive syndrome of nasal anomalies associated with renal and anorectal malformations. Clin Dysmorphol Jan 2002;11(1):33–8. 10.1097/00019605-200201000-00007. [PubMed: 11822703]
36. Fryns JP. Micro-ablepharon of the upper eyelids and vaginal atresia. Genet Couns 2001;12(1):101–2. [PubMed: 11332973]
37. Roessler E, Belloni E, Gaudenz K, et al. Mutations in the human Sonic Hedgehog gene cause holoprosencephaly. Nat Genet Nov 1996;14(3):357–60. 10.1038/ng1196-357. [PubMed: 8896572]
38. Solomon BD, Mercier S, Vélez JI, et al. Analysis of genotype-phenotype correlations in human holoprosencephaly. American journal of medical genetics Part C, Seminars in medical genetics 2010;154C(1):133–141. 10.1002/ajmg.c.30240. [PubMed: 20104608]
39. Solomon BD, Pineda-Alvarez DE, Mercier S, Raam MS, Odent S, Muenke M. Holoprosencephaly flashcards: A summary for the clinician. Am J Med Genet C Semin Med Genet Feb 2010;154C(1):3–7. 10.1002/ajmg.c.30245. [PubMed: 20104594]
40. Zhao H, Feng J, Ho TV, Grimes W, Urata M, Chai Y. The suture provides a niche for mesenchymal stem cells of craniofacial bones. Nat Cell Biol Apr 2015;17(4):386–96. 10.1038/ncb3139. [PubMed: 25799059]
41. Heyne GW, Everson JL, Ansen-Wilson LJ, et al. Gli2 gene-environment interactions contribute to the etiological complexity of holoprosencephaly: evidence from a mouse model. Dis Model Mech Nov 2016;9(11):1307–1315. 10.1242/dmm.026328. [PubMed: 27585885]
42. Kantarci S, Ackerman KG, Russell MK, et al. Characterization of the chromosome 1q41q42.12 region, and the candidate gene DISP1, in patients with CDH. Am J Med Genet A Oct 2010;152A(10):2493–504. 10.1002/ajmg.a.33618. [PubMed: 20799323]
43. Beck TF, Veenma D, Shchelochkov OA, et al. Deficiency of FRAS1-related extracellular matrix 1 (FREM1) causes congenital diaphragmatic hernia in humans and mice. Hum Mol Genet Mar 01 2013;22(5):1026–38. 10.1093/hmg/dds507. [PubMed: 23221805]
44. Mo R, Kim JH, Zhang J, Chiang C, Hui CC, Kim PC. Anorectal malformations caused by defects in sonic hedgehog signaling. Am J Pathol Aug 2001;159(2):765–74. 10.1016/S0002-9440(10)61747-6. [PubMed: 11485934]
45. Abe Y, Tanaka N. Roles of the Hedgehog Signaling Pathway in Epidermal and Hair Follicle Development, Homeostasis, and Cancer. J Dev Biol Nov 20 2017;5(4). 10.3390/jdb5040012.
46. St-Jacques B, Dassule HR, Karavanova I, et al. Sonic hedgehog signaling is essential for hair development. Curr Biol Sep 24 1998;8(19):1058–68. 10.1016/s0960-9822(98)70443-9. [PubMed: 9768360]

Author Manuscript Author Manuscript Author Manuscript Author Manuscript

47. Kiyozumi D, Yaguchi S, Yaguchi J, Yamazaki A, Sekiguchi K. Human disease-associated extracellular matrix orthologs ECM3 and QBRICK regulate primary mesenchymal cell migration in sea urchin embryos. Exp Anim Aug 06 2021;70(3):378–386. 10.1538/expanim.21-0001. [PubMed: 33828019]
48. Fitriasari S, Trainor PA. Diabetes, Oxidative Stress, and DNA Damage Modulate Cranial Neural Crest Cell Development and the Phenotype Variability of Craniofacial Disorders. Front Cell Dev Biol 2021;9:644410. 10.3389/fcell.2021.644410. [PubMed: 34095113]
49. Wu Y, Kurosaka H, Wang Q, et al. Retinoic Acid Deficiency Underlies the Etiology of Midfacial Defects. J Dent Res Jun 2022;101(6):686–694. 10.1177/00220345211062049. [PubMed: 35001679]
50. Heyne GW, Plisch EH, Melberg CG, Sandgren EP, Peter JA, Lipinski RJ. A Simple and Reliable Method for Early Pregnancy Detection in Inbred Mice. J Am Assoc Lab Anim Sci 2015;54(4):368–71. https://doi.orgn/a. [PubMed: 26224435]
51. Li H, Williams T. Separation of mouse embryonic facial ectoderm and mesenchyme. J Vis Exp Apr 2013;(74). 10.3791/50248.
52. Lopez-Rios J, Duchesne A, Speziale D, et al. Attenuated sensing of SHH by Ptch1 underlies evolution of bovine limbs. Nature Jul 03 2014;511(7507):46–51. 10.1038/nature13289. [PubMed: 24990743]
53. Li H, Durbin R. Fast and accurate short read alignment with Burrows-Wheeler transform. Bioinformatics Jul 15 2009;25(14):1754–60. 10.1093/bioinformatics/btp324. [PubMed: 19451168]
54. Quinlan AR, Hall IM. BEDTools: a flexible suite of utilities for comparing genomic features. Bioinformatics Mar 15 2010;26(6):841–2. 10.1093/bioinformatics/btq033. [PubMed: 20110278]
55. Robinson JT, Thorvaldsdóttir H, Winckler W, et al. Integrative genomics viewer. Nat Biotechnol Jan 2011;29(1):24–6. 10.1038/nbt.1754. [PubMed: 21221095]
56. O'Leary NA, Wright MW, Brister JR, et al. Reference sequence (RefSeq) database at NCBI: current status, taxonomic expansion, and functional annotation. Nucleic Acids Res Jan 04 2016;44(D1):D733–45. 10.1093/nar/gkv1189. [PubMed: 26553804]

Author Manuscript Author Manuscript Author Manuscript Author Manuscript

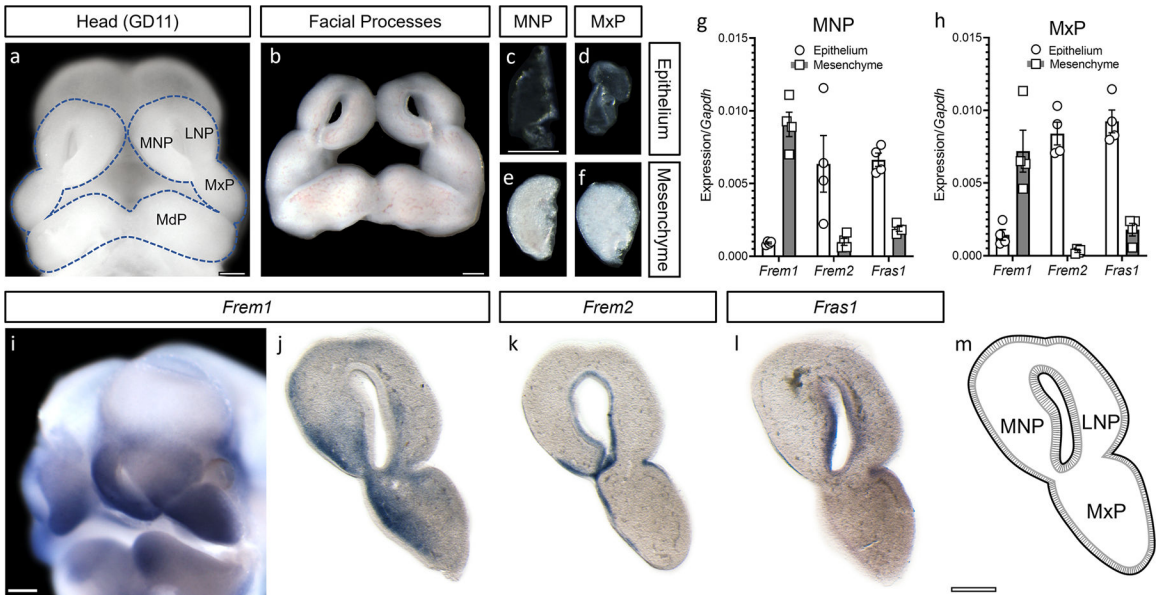

Figure 1. *Frem1* is expressed in the cNCC mesenchyme during midfacial morphogenesis.

The bilaterally paired facial growth centers that form the midface are shown in an intact GD11.0 embryo (a), after microdissection (b), and after enzymatic digestion to separate the ectodermal epithelium and cNCC-derived mesenchyme (c-f). Gene expression in epithelial and mesenchymal compartments of GD11 MNP and MxP tissue was determined by qPCR (g-h). Individual values are plotted along with the mean ± SEM of four independently collected and pooled tissue samples. Whole-mount tissue (i) and sections through the facial growth centers (j-l) were stained by ISH to visualize expression of *Frem1* (i-j), *Frem2* (k), and *Fras1* (l). At GD11, the facial growth centers fuse to form a lambdoidal junction as shown in schematic (m). MNP, medial nasal process; MxP, maxillary process; LNP, lateral nasal process; MdP, mandibular process. Scale bars: 0.25 mm.

Author Manuscript Author Manuscript Author Manuscript Author Manuscript

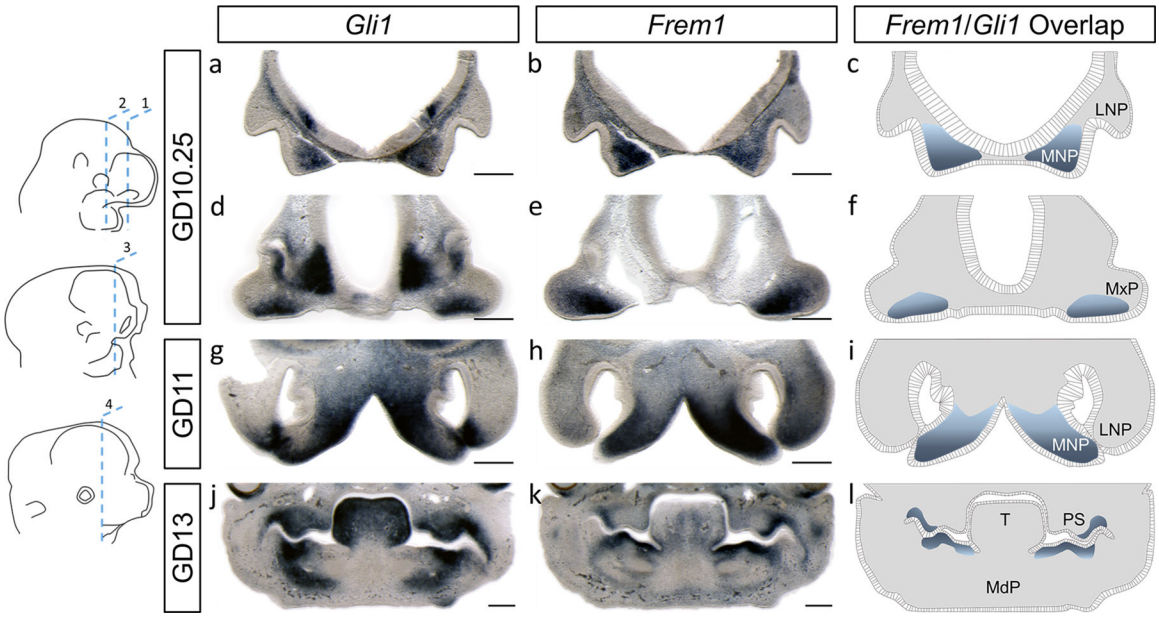

Figure 2. *Frem1* expression overlaps with Shh pathway target *Gli1* during midfacial morphogenesis.

The spatial expression of *Frem1* and *Gli1* was assessed by ISH at key stages of midfacial morphogenesis. Embryonic stages and planes of section are depicted by schematics in the left column. GD10.25 embryos were sectioned to visualize nascent MNP, LNP (a-c, plane of section 1), or MxP tissues (d-f, plane of section 2). GD11 embryos were sectioned to visualize MNP and LNP tissues along their proximal to distal axes (g-i, plane of section 3). GD13 embryos were sectioned to visualize the MxP-derived palatal shelves situated vertically along the sides of the tongue (j-l, plane of section 4). Staining is shown on adjacent sections for each stage/plane of section. Areas of apparent overlap in *Gli1* and *Frem1* expression are shown in schematics (c,f,i,l). MNP, medial nasal process; MxP, maxillary process; LNP, lateral nasal process; MdP, mandibular process; T, tongue. Scale bar: 0.25 mm.

Author Manuscript Author Manuscript Author Manuscript Author Manuscript

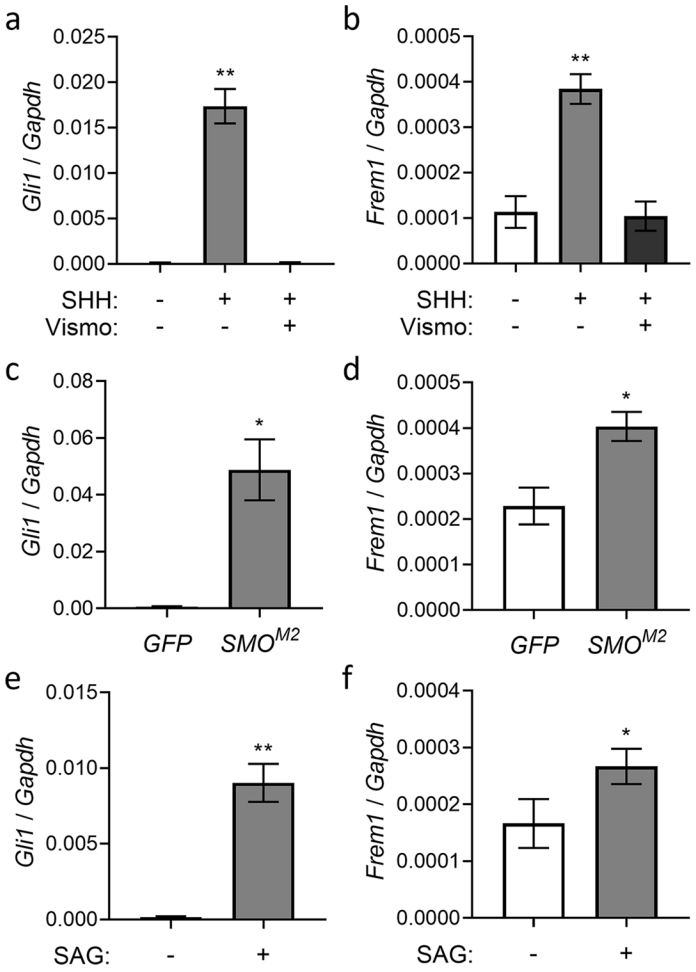

Figure 3. *Frem1* is regulated by the Shh pathway in cNCCs.

cNCCs were cultured with or without SHH ligand (0.4 μg/mL) and with or without the Smoothened antagonist vismodegib (Vismo, 100 nM) (a-b). SHH ligand caused an increase in *Gli1* and *Frem1* expression, which was blocked by the addition of vismodegib. Expression of *Gli1* and *Frem1* are increased in cNCCs expressing a constitutively active form of human Smoothened (SMO^{M2}) relative to a GFP expressing line (c-d). cNCCs cultured with the Smoothened agonist SAG (50 nM) similarly demonstrated increased expression of *Gli1* and *Frem1* compared to vehicle alone (e-f). Values represent the mean ± SEM of N=5 biological replicates for each condition. *p<0.05, ** p<0.01 (ANOVA with Tukey's post hoc test or two-tailed t-test).

Author Manuscript Author Manuscript Author Manuscript Author Manuscript

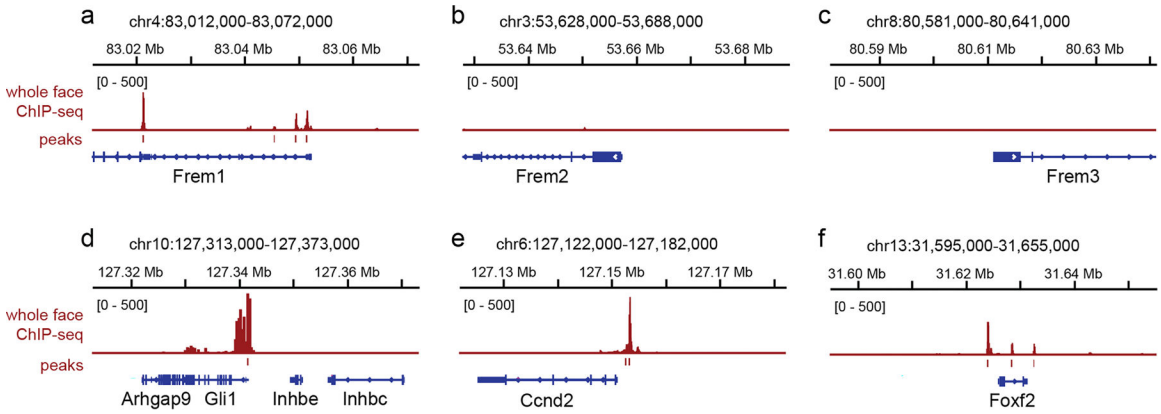

Figure 4. GLI binding to the *Frem1* promoter during facial morphogenesis.

GLI3 ChIP-seq data from GD11.5 whole face (MNP, MxP, LNP, MdP, blue tracks) were analyzed for GLI3 binding at Shh pathway target genes. GLI3 peaks (rectangles below ChIP-seq tracks) were present at both RefSeq [56] annotated transcription start sites for *Frem1* (a) but not *Frem2* (b) or *Frem3* (c). GLI3 ChIP-seq signal at the *Frem1* promoters was comparable to GLI3 signal at the promoters of known Shh targets *Gli1*, *Ccnd2,* and *Foxf2* (d-f).

Author Manuscript Author Manuscript Author Manuscript Author Manuscript

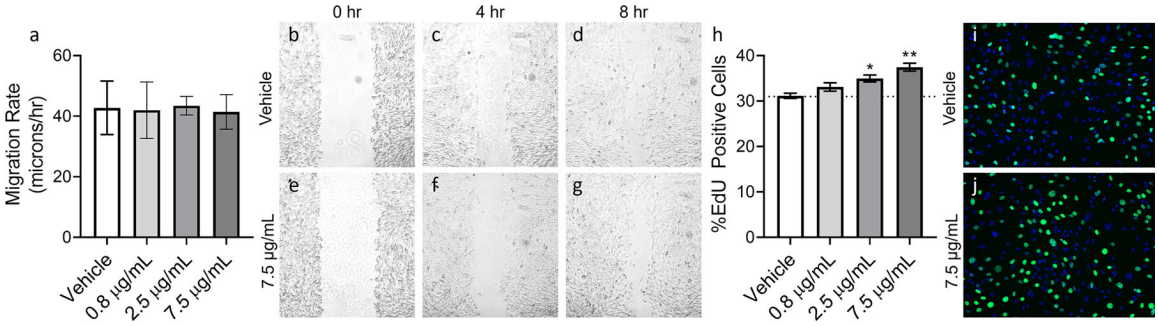

Figure 5. FREM1 promotes concentration-dependent cNCC proliferation.

Scratch assays were performed on O9–1 cells ± recombinant FREM1, and migration rate was determined over the period of scratch closure for up to 8 hours. FREM1 had no impact on the rate of O9–1 cell migration at any concentration tested (a). Representative images from vehicle- and 7.5 µg/mL FREM1-treated cells show scratch closure over time (b-g). EdU incorporation was used to assess cell proliferation in FREM1-treated O9–1 cells. Addition of recombinant FREM1 protein to culture media increased proliferation in a concentration-dependent manner (h). Representative images of vehicle- and FREM1-treated O9–1 cells stained with Hoechst (blue) and EdU (green) (i-j). Values represent the mean ± SEM of N=3 biological replicates for each condition. *$p<0.05$, **$p<0.01$ (one-way ANOVA).

Author Manuscript Author Manuscript Author Manuscript Author Manuscript

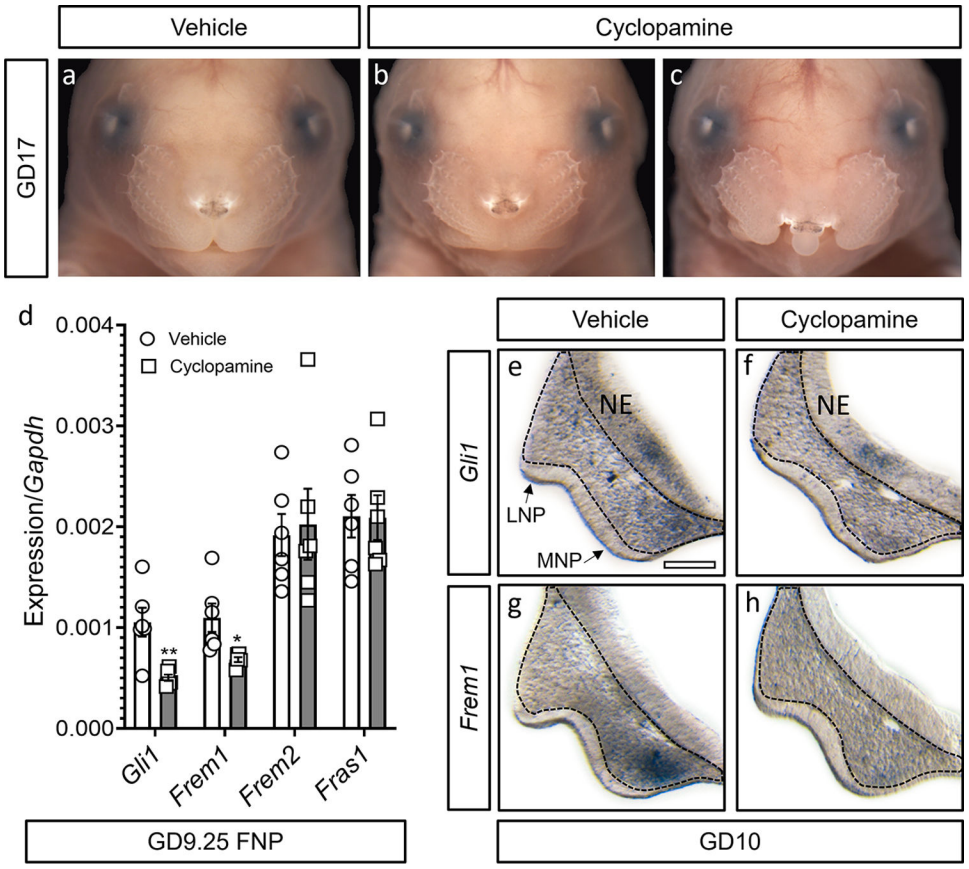

Figure 6. *Frem1* expression is diminished by Shh pathway inhibition during pathogenesis of midfacial hypoplasia/cleft lip.

In utero exposure to the Shh pathway antagonist cyclopamine from GD8.25 to 9.5 disrupts midfacial morphogenesis, resulting in either midfacial hypoplasia (b) or cleft lip (c) compared to control (a), as shown at GD17. Frontonasal prominence (FNP) tissue that gives rise to the MNPs and LNPs was microdissected from vehicle- and cyclopamine-exposed embryos at GD9.25, and gene expression was determined by qPCR (d). Expression data from pooled tissue of an entire litter are shown as individual points along with mean ± SEM. Expression of both *Gli1* and *Frem1* was significantly reduced in FNP tissue from embryos exposed to cyclopamine versus vehicle alone. * $p<0.05$, ** $p<0.01$ (two-tailed t-test). Sections through MNP and LNP tissue produced from GD10 vehicle- and cyclopamine-exposed embryos were stained by ISH to visualize expression of *Gli1* (e-f) and *Frem1* (g-h). Dashed outlines surround the mesenchyme of the MNP and LNP tissues. Cyclopamine exposure reduced expression of *Gli1* and *Frem1* in the MNP mesenchyme. MNP, medial nasal process; LNP, lateral nasal process; NE, neuroectoderm. Scale bar: 0.125 mm.

Author Manuscript Author Manuscript Author Manuscript Author Manuscript

Table 1.

***In situ* hybridization primer sequences**

Gene/Direction	Sequence
Gli1-fwd	CCCTCCTCCTCTCATTCCAC
Gli1-rev + **T7 leader**	**CGATGTTAATACGACTCACTATAGGG**TCCAGCTGAGTGTTGTCCAG
Frem1-fwd	GGACTTGAGATGGTCGTATATTG
Frem1-rev + **T7 leader**	**CGATGTTAATACGACTCACTATAGGG**GAGGATGGGAGAACTGATTTG
mFras1-fwd	CACTCTCCCATCCAGTATTTC
mFras1-rev + **T7 leader**	**CGATGTTAATACGACTCACTATAGGG**GGTGTGACCTGGTGATTATG
mFrem2-rev	GTGAACTGTCGGAACTCTAAG
mFrem2-fwd + **T7 leader**	**CGATGTTAATACGACTCACTATAGGG**CCACGACCAGAGGTAAATTC

Author Manuscript Author Manuscript Author Manuscript Author Manuscript

Table 2.

***qPCR* primer sequences**

Gene/direction	Sequence
mGapdh-fwd	AGC CTC GTC CCG TAG ACA AAA T
mGapdh-rev	CCG TGA GTG GAG TCA TAC TGG A
mGli1-fwd	GGA AGT CCT ATT CAC GCC TTG A
mGli1-rev	CAA CCT TCT TGC TCA CAC ATG TAA G
mFrem1-fwd	GGT CCC AAG GGC TGC ATT TAT
mFrem1-rev	CAA CAA GGG TTT CGG AGT CTC ATC
mFras1-fwd	TTG GCC ATC CTC TTG GAA ATC AC
mFras1-rev	TGG TAT GCG GCT TCT TCA AAC TC
mFrem2-fwd	ACT TCG AGG AAC GCC CAA ATA C
mFrem2-rev	GCA GCT CCT CTA CAT CCT CAT AGA
mItga8-fwd	CAG GCA AGG ATC AAC GAG GTA AAG
mItga8-rev	AAG CCA AAT CCA GAA GGG ATGG
mNpnt-fwd	TGC CCT CTT GTC TCC CTC TTA TC
mNpnt-rev	TGT CTC CAG ATG CTC CTG TAC TT